Inorg. Chem. **2009**, *48*, 3755−3767

Conjugated Triarylboryl Donor−Acceptor Systems Supported by 2,2′-Bipyridine: Metal Chelation Impact on Intraligand Charger Transfer Emission, Electron Accepting Ability, and "Turn-on" Fluoride Sensing

Yi Sun and Suning Wang*

Department of Chemistry, Queen's University, Kingston, Ontario K7L 3N6, Canada

Received January 8, 2009

To investigate the impact of metal-chelation on intraligand charge transfer emission involving a triarylboron group, three 2,2′-bipyridine derivative molecules, 5,5′-bis($BMes_2$)-2,2′-bipy (B2bpy), 5-($BMes_2$)-5′-(NPh_2)-2,2′-bipy (BNbpy), and 5,5′-bis(NPh_2)-2,2′-bipy (N2bpy) have been synthesized, which can be described as donor-only, donor−acceptor, and acceptor-only systems. Each of these molecules displays distinctive electrochemical and photophysical properties with BNbpy and N2bpy being bright emitters and B2bpy being a strong electron acceptor. In addition, BNbpy displays a "turn-on" fluorescent response while B2bpy has a "turn-off" response upon binding with fluoride ions. These molecules can readily chelate to a $PtPh_2$ or a $PtCl_2$ group, producing square planar complexes Pt(B2bpy)Ph_2 (**Pt-1**), Pt(B2bpy)Cl_2 (**Pt-1a**), Pt(BNbpy)Ph_2 (**Pt-2**), Pt(BNbpy)Cl_2 (**Pt-2a**), and Pt(N2bpy)Ph_2 (**Pt-3**) that have significantly altered electrochemical and photophysical properties from those of the free ligands. Metal chelation has been found to greatly enhance the electron accepting ability of the three ligands, especially B2bpy and BNbpy. The Ph and Cl auxiliary ligands have also been found to have a significant impact on the electrochemical and photophysical properties of the complexes. B2bpy complexes **Pt-1** and **Pt-1a** are not luminescent at ambient temperature while BNbpy complexes **Pt-2** and **Pt-2a** display room temperature phosphorescence in solution under air that has a similar "turn-on" response toward fluoride ions as the free BNbpy does but with a much more dramatic color switch (orange or red to blue-green). The persistent intraligand N→B charge transfer transition in the BNbpy complexes is believed to play a key role in their unique phosphorescent response toward fluorides. The complex **Pt-3** displays a bright blue-green phosphorescence in solution at ambient temperature. Density functional theory computations established that the lowest electronic transition in the Pt(II) complex is from the Pt(II) d orbital and the auxiliary ligand to the π^* orbital of the 2,2′-bipy derivative ligand.

Introduction

Conjugated three-coordinate organoboron compounds have recently emerged as an important and very promising class of materials for various photonic and optoelectronic application including nonlinear optical materials,[1] charge-transport materials, and emitters in organic light emitting devices (OLED).[2] Furthermore, three-coordinate organoboron compounds have also been shown to be effective colorimetric, fluorescent, or ratiometric sensors for the selective detection

* To whom correspondence should be addressed. E-mail: wangs@chem.queensu.ca.

(1) (a) Yuan, Z.; Taylor, N. J.; Ramachandran, R.; Marder, T. B. *Appl. Organomet. Chem.* **1996**, *10*, 305. (b) Yuan, Z.; Entwistle, C. D.; Collings, J. C.; Albesa-Jové, D.; Batsanov, A. S.; Howard, J. A. K.; Kaiser, H. M.; Kaufmann, D. E.; Poon, S.-Y; Wong, W.-Y; Jardin, C.; Fathallah, S.; Boucekkine, A.; Halet, J.-F.; Taylor, N. J.; Marder, T. B. *Chem.—Eur. J.* **2006**, *12*, 2758. (c) Entwistle, C. D.; Marder, T. B. *Angew. Chem., Int. Ed.* **2002**, *41*, 2927. (d) Entwistle, C. D.; Marder, T. B. *Chem. Mater.* **2004**, *16*, 4574. (e) Stahl, R.; Lambert, C.; Kaiser, C.; Wortmann, R.; Jakober, R. *Chem.—Eur. J.* **2006**, *12*, 2358. (f) Matsumi, N.; Chujo, Y. *Polymer J. (Tokyo, Jpn.)* **2008**, *40*, 77. (g) Lequan, M.; Lequan, R. M.; Ching, K. C. *J. Mater. Chem.* **1991**, *1*, 997. (h) Liu, Z. Q.; Fang, Q.; Cao, D. X.; Wang, D.; Xu, G. B. *Org. Lett.* **2004**, *6*, 2933. (i) Tao, L. M.; Guo, Y. H.; Huang, X. M.; Wang, C. K. *Chem. Phys. Lett.* **2006**, *425*, 10.

(2) (a) Noda, T.; Shirota, Y. *J. Am. Chem. Soc.* **1998**, *120*, 9714. (b) Shirota, Y. *J. Mater. Chem.* **2005**, *15*, 75. (c) Noda, T.; Ogawa, H.; Shirota, Y. *Adv. Mater.* **1999**, *11*, 283. (d) Shirota, Y.; Kinoshita, M.; Noda, T.; Okumoto, K.; Ohara, T. *J. Am. Chem. Soc.* **2000**, *122*, 1102. (e) Jia, W. L.; Bai, D. R.; McCormick, T.; Liu, Q. D.; Motala, M.; Wang, R.; Seward, C.; Tao, Y.; Wang, S. *Chem.—Eur. J.* **2004**, *10*, 994. (f) Jia, W. L.; Moran, M. J.; Yuan, Y. Y.; Lu, Z. H.; Wang, S. *J. Mater. Chem.* **2005**, *15*, 3326. (g) Jia, W. L.; Feng, X. D.; Bai, D. R.; Lu, Z. H.; Wang, S.; Vamvounis, G. *Chem. Mater.* **2005**, *17*, 164. (h) Li, F. H.; Jia, W. L.; Wang, S.; Zhao, Y. Q.; Lu, Z. H. *J. Appl. Phys.* **2008**, *103*, 034509/1–034509/6. (i) Wakamiya, A.; Mori, K.; Yamaguchi, S. *Angew. Chem., Int. Ed.* **2007**, *46*, 4237.

10.1021/ic9000335 CCC: $40.75
Published on Web 03/03/2009

of anions such as fluorides and cyanides[3,4] and for the activation of molecular hydrogen molecules[5] by utilizing the empty p_π orbital on the boron center. To be effective for either OLEDs or sensor applications, it is necessary for the triarylboron compound to have high emission quantum efficiency and strong electron accepting ability or Lewis acidity. Donor−acceptor systems involving a triarylboron group have been shown to be particularly effective as either bright emitters for OLEDs or as fluorescent sensors for anions.[5] Previous studies have established that the direct conjugation of a donor and an acceptor via an aromatic linker in a triarylboron compound can greatly enhance the quantum efficiency of the donor to acceptor charge transfer emission.[4d−f] Although many π-conjugated donor−acceptor triarylboron compounds have been reported recently, they typically involve non-coordinating aromatic linkers such as phenyl, biphenyl, and thienyl with an electron accepting ability/Lewis acidity comparable to that of a typical triarylboron compound such as $BMes_3$ (Mes = mesityl).[2−4] A number of Ir(III) complexes with N,C-chelating phenylpyridine (ppy) and derivative ligands functionalized by a $BMes_2$ group have been shown recently to be effective phosphorescent emitters in OLEDs[6a] and sensors for fluoride ions,[6b,c] although the role of the B center in phosphorescence is not clear because of the highly emissive nature of the Ir^{III}-ppy chromophore. By investigating Pt(II) and Cu(I) complexes, we have shown that a $BMes_2$ functionalized N,N-chelate ligand (*N*-2-(5-$BMes_2$)pyridyl)-7-azaindole, BNPA) can greatly facilitate metal to ligand charge transfer (MLCT) emission in the complexes, compared to the non-functionalized NPA ligand.[7] We have also demonstrated that the 2,2′-bipy ligand is an excellent linker for two $BMes_2$, and the resulting 5,5′-bis($BMes_2$)-2,2′-bipy (B2bpy) molecule has a high electron accepting ability and a strong binding constant with F^-.[8] Furthermore, we have shown that by chelating to either a $Pt^{II}R_2$ (R = Me, Ph) or a $[Cu^I(PPh_3)_2]^+$ unit, the Lewis acidity/electron accepting ability of the boron centers can be further enhanced.[8] Most significant is that the Pt(II) or Cu(I) complexes of B2bpy display distinct MLCT absorption bands in the visible region that can be quenched by the addition of fluoride ions, thus allowing the detection of fluoride ions via visual color change. Nonetheless, the acceptor-only B2bpy molecule has a very low fluorescent quantum efficiency (1%) and its Pt(II) and Cu(I) complexes are not emissive in solution at ambient temperature; hence, they are not suitable as emitters for OLEDs and not very effective for sensing fluorides in the fluorescent mode. To enhance the luminescent efficiency and to examine the impact of metal chelation on Lewis acidity and electron accepting ability of donor−acceptor chelate molecules, we have investigated a new donor−acceptor molecule BNbpy shown in Scheme 1. To fully understand the impact of the three-coordinate boron center on the photophysical properties of B2bpy and BNbpy and their metal complexes, we also investigated the donor-only molecule, N2bpy. The results of our comprehensive investigation on B2bpy, BNbpy, N2bpy, and their corresponding Pt(II) complexes are presented herein.

Experimental Section

All reactions were performed under an inert atmosphere of dry N_2 with standard Schlenk techniques unless otherwise noted. All starting materials were purchased from Aldrich Chemical Co. and used without further purification. Tetrahydrofuran (THF), toluene, and CH_2Cl_2 were purified using the solvent purification system (Innovation Technologies Co.). Deuterated solvents from Cambridge Isotopes were used as received without further drying. NMR spectra were recorded on a Bruker Avance 400 spectrometer (400.13 MHz for ^1H, 100.62 MHz for ^{13}C, 376.50 MHz for ^{19}F), chemical shifts are referenced to the residual solvent peaks and have been reported in parts per million (ppm) relative to TMS (^1H and ^{13}C) and $CFCl_3$ (^{19}F). UV−vis spectra were recorded on an Ocean Optics USB2000+ spectrophotometer. Cyclic voltammetry was performed using a BAS CV-50W analyzer with a scan rate of 100 mV/s to 1 V/s and a typical concentration of 5 mg of the compounds in 3 mL of dimethylformamide (DMF). The electrolytic cell used was a conventional three-compartment cell, in which a Pt working electrode, a Pt auxiliary electrode, and a Ag/AgCl reference electrode were employed. The CV measurements were performed at room temperature using 0.10 M NBu_4PF_6 as the supporting electrolyte and DMF as the solvent. The ferrocenium/ferrocene couple was used as the standard ($E_0 = 0.55$ V). Elemental analyses were performed at Canadian Microanalytical Service, Delta, British Columbia. 5,5′-Dibromo-2,2′-bipyridine,[9] 5,5′-bis($BMes_2$)-2,2′-bipyridine (B2bpy),[8] $[PtPh_2(SMe_2)]_n$ ($n = 2$ or 3),[10] and Pt(B2bpy)Ph_2 (**1**)[8] were prepared by modified methods described in the literature.

(3) (a) Yamaguchi, S.; Shirasaka, T.; Akiyama, S.; Tamao, K. *J. Am. Chem. Soc.* **2002**, *124*, 8816. (b) Yamaguchi, S.; Akiyama, S.; Tamao, K. *J. Am. Chem. Soc.* **2001**, *123*, 11372. (c) Solé, S.; Gabbaï, F. P. *Chem. Commun.* **2004**, 1284. (d) Melaimi, M.; Gabbaï, F. P. *J. Am. Chem. Soc.* **2005**, *127*, 9680. (e) Chiu, C. W.; Gabbaï, F. P. *J. Am. Chem. Soc.* **2006**, *128*, 14248. (f) Hudnall, T. W.; Melaimi, M.; Gabbaï, F. P. *Org. Lett.* **2006**, *8*, 2747. (g) Lee, M. H.; Agou, T.; Kobayashi, J.; Kawashima, T.; Gabbaï, F. P. *Chem. Commun.* **2007**, 1133. (h) Lee, M. H.; Gabbaï, F. P. *Inorg. Chem.* **2007**, *46*, 8132. (i) Hudnall, T. W.; Gabbaï, F. P. *J. Am. Chem. Soc.* **2007**, *129*, 11978. (k) Dorsey, C. L.; Jewula, P.; Hudnall, T. W.; Hoefelmeyer, J. D.; Taylor, T. J.; Honesty, N. R.; Chiu, C.-W.; Schulte, M.; Gabbaï, F. P. *Dalton Trans.* **2008**, 4442. (l) Hudnall, T. W.; Kim, Y.-M.; Bebbington, M. W. P.; Bourissou, D.; Gabbaï, F. P. *J. Am. Chem. Soc.* **2008**, *130*, 10890.

(4) (a) Sundararaman, A.; Venkatasubbaiah, K.; Victor, M.; Zakharov, L. N.; Rheingold, A. L.; Jäkle, F. *J. Am. Chem. Soc.* **2006**, *128*, 16554. (b) Parab, K.; Venkatasubbaiah, K.; Jäkle, F. *J. Am. Chem. Soc.* **2006**, *128*, 12879. (c) Jäkle, F. *Coord. Chem. Rev.* **2006**, *250*, 1107. (d) Liu, X. Y.; Bai, D. R.; Wang, S. *Angew. Chem., Int. Ed.* **2006**, *45*, 5475. (e) Bai, D. R.; Liu, X. Y.; Wang, S. *Chem.−Eur. J.* **2007**, *13*, 5713. (f) Zhao, S. B.; Wucher, P.; Hudson, Z. M; Mc Cormick, T. M.; Liu, X. Y.; Wang, S.; Feng, X. D.; Lu, Z. H. *Organometallics* **2008**, *27*, 6446. (g) Zhou, G.; Baumgarten, M.; Müllen, K. *J. Am. Chem. Soc.* **2008**, *130*, 12477.

(5) (a) Welch, G. C.; San Juan, R. R.; Masuda, J. D.; Stephan, D. W. *Science* **2006**, *314*, 1124. (b) Welch, G. C.; Stephan, D. W. *J. Am. Chem. Soc.* **2007**, *129*, 1880. (c) Chase, P. A.; Welch, G. C.; Jurca, T.; Stephan, D. W. *Angew. Chem., Int. Ed.* **2007**, *46*, 8050. (d) Geier, S. J.; Gilbert, T. M.; Stephan, D. W. *J. Am. Chem. Soc.* **2008**, *130*, 12632.

(6) (a) Zhou, G. J.; Ho, C. L.; Wong, W. Y.; Wang, Q.; Ma, D. G.; Wang, L. X.; Lin, Z. Y.; Marder, T. B.; Beeby, A. *Adv. Funct. Mater.* **2008**, *18*, 499. (b) You, Y. M.; Park, S. Y. *Adv. Mater.* **2008**, *20*, 3820. (c) Zhao, Q.; Li, F. Y.; Liu, S. J.; Yu, M. X.; Liu, Z. Q.; Yi, T.; Huang, C. H. *Inorg. Chem.* **2008**, *47*, 9256.

(7) Zhao, S. B.; McCormick, T.; Wang, S. *Inorg. Chem.* **2007**, *46*, 10965.

(8) Sun, Y.; Ross, N.; Zhao, S.-B.; Huszarik, K.; Jia, W. L.; Wang, R. Y.; Wang, S. *J. Am. Chem. Soc.* **2007**, *129*, 7510.

(9) Liu, S.-J.; Zhao, Q.; Chen, R.-F.; Deng, Y.; Fan, Q.-L.; Li, F.-Y.; Wang, L.-H.; Huang, C.-H.; Huang, W. *Chem.−Eur. J.* **2006**, *12*, 4351.

(10) (a) Song, D.; Wang, S. *J. Organomet. Chem.* **2002**, *648*, 302. (b) Scott, J. D.; Puddephatt, R. J. *Organometallics* **1983**, *2*, 1643.

Scheme 1

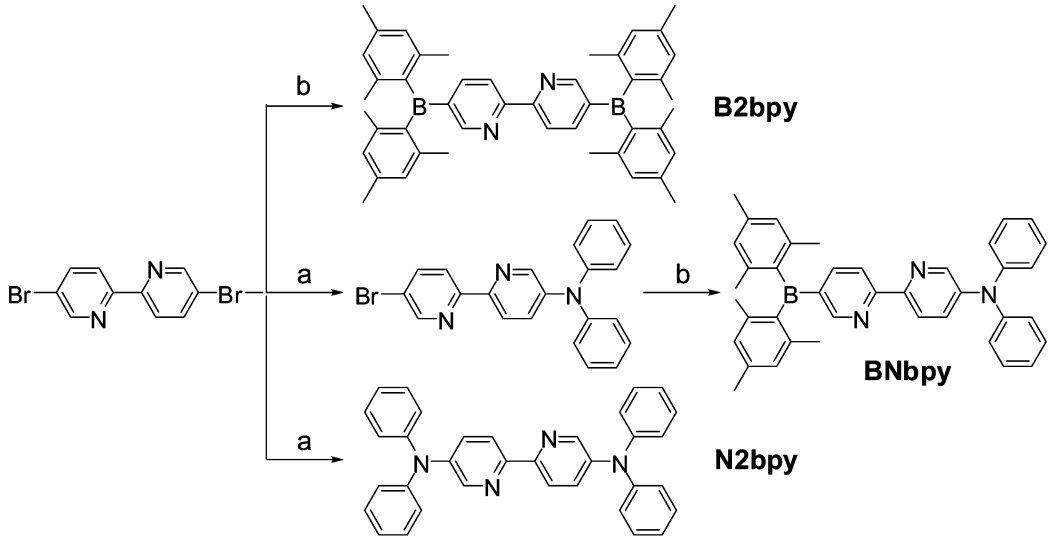

a) diphenyl amine, $Pd_2(dba)_3$, Binap, $NaOBu^t$, Toluene, 100°C.
b) *n*-BuLi, $FB(Mes)_2$, THF, -100°C.

Synthesis of 5-Bromo-5′-diphenylamino-bipyridine (Br-bpy-NPh$_2$). A mixture of 5,5′-dibromo-2,2′-bipyridine (314 mg, 1.0 mmol) and diphenylamine (115 mg, 0.67 mmol) was dissolved in toluene (10 mL). Sodium-*tert*-butoxide (90 mg, 0.90 mmol), tri(dibenzylideneacetone)dipalladium(0) ($Pd_2(dba)_3$) (12 mg, 0.013 mmol), and 2,2′-bis(diphenylphosphino)-1,1′-binaphthyl (±BINAP) (17 mg, 0.026 mmol) were added to the solution. The reaction mixture was stirred at 100 °C for 16 h under nitrogen. After cooling to room temperature, the mixture was quenched by the addition of an aqueous solution of EDTA, and the product was extracted with CH_2Cl_2. The crude product was purified by column chromatography on silica gel (hexane/ether acetyl, 30/1) to afford light yellow solid of the product, 81 mg in 30% yield. ^{1}H NMR (400 MHz, $CDCl_3$): 8.66 (d, J = 1.5 Hz, 1H, py), 8.37 (d, J = 1.5 Hz, 1H, py), 8.20 (dd, J = 2.1 Hz, J = 6.3 Hz, 2H, py), 7.87 (dd, J = 1.5 Hz, J = 6.3 Hz, 1H, py), 7.44 (dd, J = 1.5 Hz, J = 6.3 Hz, 1H, py), 7.31 (t, J = 5.7 Hz, 4H, ph), 7.13 (m, 6H, ph). ^{13} C NMR (100 MHz, $CDCl_3$): 154.9, 150.3, 148.1, 146.9, 145.2, 143.4, 139.6, 131.3, 130.0, 129.2, 125.3, 124.6, 121.9, 121.3, 120.3 (aryl *C*). HRMS: calcd for $C_{22}H_{16}N_3Br$, $[M]^+$: 401.0528; found: 401.0518.

Synthesis of BNbpy. To a solution of Br-bpy-NPh$_2$ (100 mg, 0.25 mmol) in THF (50 mL) was added a hexane solution of *n*-BuLi (1.6 M, 0.17 mL, 0.28 mmol) at −100 °C, and the mixture was stirred for 1 h at this temperature. Then a solution of dimesitylboron fluoride (82 mg, 90%, 0.28 mmol) in THF (10 mL) was added. The reaction mixture was stirred for another 1 h at −100 °C, allowed to slowly reach room temperature, and kept stirring overnight. Solvents were removed under reduced pressure. The residue was subjected to column chromatography on silica gel (hexane/ether acetyl, 25:1) to afford BNbpy (91 mg, 64% yield). Mp 80 °C. ^{1}H NMR (400 MHz, CD_2Cl_2): 8.60 (m, 1H, py), 8.35 (d, J = 1.5 Hz, 1H, py), 8.32 (dd, J = 0.8 Hz, J = 8.8 Hz, 1H, py), 8.29 (d, J = 1.2 Hz, J = 8.0 Hz, 1H, py), 7.80 (dd, J = 1.5 Hz, J = 8.0 Hz, 1H, py), 7.42 (d, J = 2.1 Hz, J = 8.8 Hz, 1H, py), 7.33 (t, J = 5.7 Hz, 4H, Ph), 7.13 (m, 6H, Ph), 6.85 (s, 4H, Mes), 2.29 (s, 6H, Me), 2.03 (s, 12H, Me). ^{13}C NMR (100 MHz, CD_2Cl_2): 159.7, 158.6, 156.0, 150.1, 148.9, 146.9, 145.4, 144.7, 143.5, 141.1, 139.6, 130.0, 128.9, 128.7, 125.4, 124.6, 122.1, 119.9 (aryl C), 23.6, 21.3 (*C*H$_3$ of Mes). HRMS: calcd for $C_{40}H_{38}BN_3$, $[M]^+$: 571.3159; found: 571.3166.

Synthesis of N2bpy. A mixture of 5,5′-dibromo-2,2′-bipyridine (157 mg, 0.50 mmol) and diphenylamine (203 mg, 1.20 mmol) was dissolved in toluene (10 mL). Sodium-*tert*-butoxide (115 mg, 1.20 mmol), $Pd_2(dba)_3$ (9.5 mg, 0.010 mmol) and (±)BINAP (13 mg, 0.020 mmol) were added to the solution. The reaction mixture was stirred at 100 °C for 24 h under the nitrogen. After cooling to room temperature, the mixture was quenched by the addition of an aqueous solution of EDTA, and the product was extracted with CH_2Cl_2. The crude product was purified by column chromatography on silica gel (hexane/THF, 10/1) to afford light yellow solid of N2bpy, 113 mg in 46% yield. Mp 125 °C. ^{1}H NMR (400 MHz, $CDCl_3$): 8.37 (d, J = 2.4 Hz, 2H, py), 8.15 (d, J = 6.9 Hz, 2H, py), 7.45 (dd, J = 2.7 Hz, J = 8.7 Hz, 2H, py), 7.30 (m, 8H, Ph), 7.10 (m, 12H, Ph). ^{13} C NMR (100 MHz, $CDCl_3$): 146.7, 143.8, 129.9, 129.6, 124.6, 123.8, 120.6 (aryl *C*). HRMS: calcd for $C_{34}H_{26}N_4$, $[M]^+$: 490.2157; found: 490.2148.

Synthesis of Pt(BNbpy)Ph$_2$ (2). BNbpy (57 mg, 0.10 mmol) and $[PtPh_2(\mu\text{-}SMe_2)]_n$ (n = 2 or 3, 41 mg, 0.10 mmol) were mixed in 20 mL of CH_2Cl_2 and stirred for 12 h under nitrogen at room temperature. After removal of solvent, the red residue was washed by Et_2O (10 mL) and dried under vacuum to afford **2** in 87% yield. ^{1}H NMR (400 MHz, CD_2Cl_2): 8.33 (s, 1H, py), 8.20 (d, J = 2.5 Hz, 1H, py), 7.98 (dd, J = 1.5 Hz, J = 8.0 Hz, 1H, py), 7.86 (d, J = 9.0 Hz, 1H, py), 7.84 (d, J = 8.0 Hz, 1H, py), 7.50 (dd, J = 2.5 Hz, J = 9.0 Hz, 1H, py), 7.34 (t, J = 8.0 Hz, 4H, N-Ph), 7.21 (t, J = 7.5 Hz, 4H, N-Ph), 7.14 (m, 2H, N-Ph), 7.08 (d, satellite, J = 7.5 Hz, J_{Pt-H} = 62.5 Hz, 4H, Pt-Ph), 6.80 (s, 4H, Mes), 6.63 (m, 4H, Pt-Ph), 6.56 (m, 2H, Pt-Ph), 2.32 (s, 6H, Me), 1.94 (s, 12H, Me). ^{13}C NMR (100 MHz, CD_2Cl_2): 158.1, 156.7, 145.1, 144.6, 140.8, 140.0, 138.9, 138.1, 138.0, 130.5, 128.9, 127.2, 126.2, 125.2, 123.7, 121.7, 120.5 (aryl *C*), 23.7, 21.3 (Me). Anal. Calcd for $C_{52}H_{48}BN_3Pt$: C, 67.82; H, 5.25; N, 4.56. Found: C, 67.75; H, 4.92; N, 4.10.

Synthesis of Pt(N2bpy)Ph$_2$ (3). N2bpy (49 mg, 0.10 mmol) and $[PtPh_2(\mu\text{-}SMe_2)]_n$ (n = 2 or 3, 41 mg, 0.10 mmol) were mixed in 20 mL of CH_2Cl_2 and stirred for 12 h under the nitrogen at room temperature. After removal of solvent, the yellow residue was washed by Et_2O (10 mL) and dried under vacuum to afford **3** in 82% yield. ^{1}H NMR (400 MHz, CD_2Cl_2): 8.11 (d, J = 2.4 Hz, 2H, py), 7.65 (d, J = 8.8 Hz, 2H, py), 7.51 (dd, J = 2.4 Hz, J = 8.8

Hz, 2H, py), 7.32 (t, $J = 7.8$ Hz, 4H, N-Ph), 7.21 (m, 4H, N-Ph), 7.13 (m, 2H, N-Ph), 7.06 (dd, satellite, $J = 0.8$ Hz, $J = 7.5$ Hz, $J_{Pt-H} = 49.6$ Hz, 4H, Pt-Ph), 6.61 (m, 4H, Pt-Ph), 6.53 (m, 2H, Pt-Ph). ^{13}C NMR (100 MHz, CD_2Cl_2): 150.7, 149.5, 145.7, 143.9, 143.1, 142.6, 142.5, 138.4, 138.2, 131.4, 130.3, 127.2, 126.8, 125.8, 121.6 (aryl *C*). Anal. Calcd for $C_{36}H_{36}N_4Pt$: C, 65.78; H, 4.32; N, 6.67. Found: C, 65.77; H, 4.41; N, 6.16.

Synthesis of Pt(B2bpy)Cl$_2$ (1a). To a stirred solution of K_2PtCl_4 (41.5 mg, 0.10 mmol) in mixed solvent H_2O (10 mL) and DMSO (0.5 mL) was added B2bpy (65.3 mg, 0.10 mmol) in CH_2Cl_2 (5 mL). The mixture was stirred at room temperature for 6 h. When the color of the water phase disappeared, the yellow organic phase was separated. The product was precipitated by hexane (20 mL) and washed by diethyl ether to afford yellow powder of **1a**, 77 mg in 84% yield. ^{1}H NMR (400 MHz, CD_2Cl_2): 9.73 (d, $J = 1.2$ Hz, 2H, py), 8.14 (dd, $J = 1.2$ Hz, $J = 8.0$ Hz, 2H, py), 7.96 (d, $J = 8.0$ Hz, 2H, py), 6.91 (s, 8H, Mes), 2.34 (s, 6H, Me), 2.07 (s, 12H, Me). ^{13}C NMR (100 MHz, CD_2Cl_2): 162.7, 162.3, 158.3, 156.0, 147.1, 145.3, 141.5, 141.2, 140.0, 138.0, 129.3, 127.2, 123.1, 116.4, 113.6 (aryl *C*), 23.8, 21.3 (Me). Anal. Calcd for $C_{46}H_{50}B_2Cl_2N_2Pt$: C, 60.15; H, 5.49; N, 3.05. Found: C, 60.35; H, 5.66; N, 2.75.

Synthesis of Pt(BNbpy)Cl$_2$ (2a). To a stirred solution of K_2PtCl_4 (20.6 mg, 0.05 mmol) in mixed solvent H_2O (5 mL) and DMSO (0.2 mL) was added BNbpy (28.6 mg, 0.05 mmol) in CH_2Cl_2 (5 mL). The mixture was stirred at room temperature for 6 h. When the color of water phase disappeared, the orange organic phase was separated. The product was precipitated by hexane (20 mL) and washed by diethyl ether to afford orange powder of **2a**, 33 mg in 78% yield. ^{1}H NMR (400 MHz, CD_2Cl_2): 9.58 (s, 1H, py), 9.36 (d, $J = 3.0$ Hz, 1H, py), 8.02 (dd, $J = 1.8$ Hz, $J = 7.8$ Hz, 1H, py), 7.69 (d, $J = 9.0$ Hz, 1H, py), 7.67 (d, $J = 7.8$ Hz, 1H, py), 7.50 (dd, $J = 2.4$ Hz, $J = 9.0$ Hz, 1H, py), 7.47 (t, $J = 7.8$ Hz, 4H, N-Ph), 7.32 (t, $J = 7.2$ Hz, 4H, N-Ph), 7.25 (m, 2H, N-Ph), 6.90 (s, 4H, Mes), 2.32 (s, 6H, Me), 2.02 (s, 12H, Me). ^{13}C NMR (100 MHz, CD_2Cl_2): 164.0, 159.3, 156.2, 147.8, 146.2, 144.4, 141.3, 140.7, 130.7, 129,1 127.2, 126.6, 125.2, 124.0, 120.5 (aryl *C*), 23.9, 21.4 (Me).

Results and Discussion

Syntheses of Ligands and Their Pt(II) Complexes. The synthetic procedures for B2bpy, BNbpy, and N2bpy are shown in Scheme 1. The starting material 5-bromo-5′-diphenylamino-bipyridine (Br-bpy-NPh$_2$) and N2bpy were synthesized by Pd-catalyzed C−N bond formation reaction of 5,5′-dibromo-2,2′-bipyridine (Br$_2$-bpy) with HNPh$_2$ in a 1:0.67 and a 1:2.4 ratio, respectively. The yields of Br-bpy-NPh$_2$ and N2bpy were found to be highly dependent on the ratio of Br$_2$-bpy and HNPh$_2$ and the catalytic systems for performing aryl amination. For the synthesis of Br-bpy-NPh$_2$, the combination of Br$_2$-bpy and HNPh$_2$ in 1.0:0.67 ratio significantly reduces the amount of the byproduct N2bpy, compared to the reaction with a 1:1 ratio. For the synthesis of N2bpy, the 1.0:2.4 ratio of Br$_2$-bpy and HNPh$_2$ gave the best yield. The mixture of Pd$_2$(dba)$_3$ and (±)BINAP (1:2) was found to be the most effective catalytic system for the synthesis of Br-bpy-NPh$_2$ and N2bpy. The effectiveness of the chelating BINAP ligand was presumably due to the fact that the chelating ligand inhibits Pd(II) binding to the bpy site. The synthesis of B2bpy and BNbpy were accomplished by the reaction of BMes$_2$F with Li$_2$(2,2′-bpy) and Li(5-NPh$_2$-2,2′-bpy), respectively, in THF at −100 °C in ∼60% yields.

Chart 1

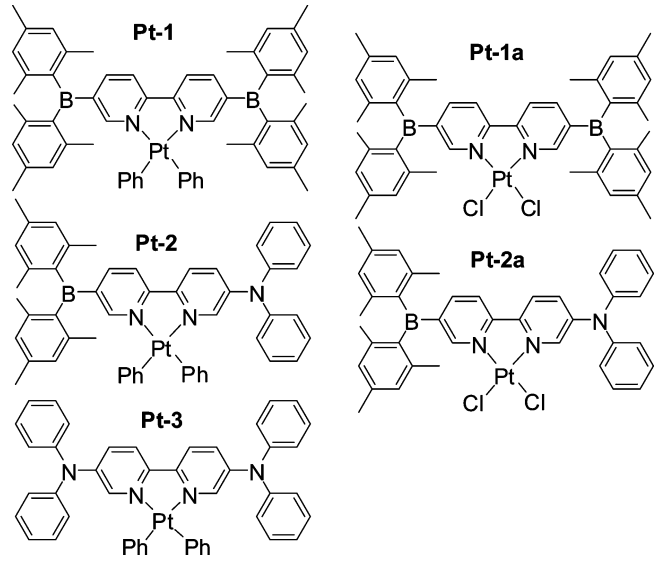

B2bpy is a white solid while BNbpy and N2bpy are both yellow solids. Like 2,2′-bpy, B2bpy, BNbpy and N2bpy are all effective chelate ligands for metal ions, and their corresponding PtPh$_2$ complexes Pt(B2bpy)Ph$_2$ (**Pt-1**), Pt(B-Nbpy)Ph$_2$ (**Pt-2**), and Pt(N2bpy)Ph$_2$ (**Pt-3**) were obtained readily by the reaction of the chelate ligand with $[PtPh_2(SMe_2)]_n$ in high yields. The PtCl$_2$ complexes Pt(B2bpy)Cl$_2$ (**Pt-1a**) and Pt(BNbpy)Cl$_2$ (**Pt-2a**) were obtained by the reaction of the chelate ligand with K_2PtCl_4. The structures of all Pt(II) complexes are shown in Chart 1. The choice of the Pt(II) ion is based on the consideration that Pt(II) diimine complexes are well-known to display metal-to-ligand (diimine) charge transfer (MLCT) transitions,[11] thus allowing us to examine the influence of the donor and acceptor groups on MLCT transitions. The three PtPh$_2$ complexes display distinct colors: **Pt-1**, red, **Pt-2**, orange, and **Pt-3**, yellow. They are all air stable in both solution and the solid state. The ligands and their Pt(II) complexes have been fully characterized by NMR spectroscopy and HR-MS or element analyses. The crystal structures of B2bpy, **Pt-1** were presented in a preliminary communication article.[8] The structure of **Pt-1a** determined by X-ray diffraction is shown in Figure 1. The Pt−N bond lengths of **Pt-1a** are much shorter (1.988(4), 1.990(14) Å) than those in **Pt-1** (2.095(2) Å) because of the much greater *trans* effect of the phenyl group. In addition, the two boron atoms in **Pt-1a** are much less out of linearity with the two pyridine rings than those in **Pt-1**, as evidenced by the B···B−C$_{py}$ angle, 6.13°, 7.98° in **Pt-1a**, 8.84° in **Pt-1**, attributable to the much reduced steric congestion in **Pt-1a**. All other Pt(II) complexes did not produce single crystals that are appropriate for X-ray diffraction analysis.

Absorption Spectra. Ligands. The absorption spectra of the free ligands B2bpy, BNbpy, and N2bpy are shown in

(11) (a) Wadas, T. J.; Chakraborty, S.; Lachicotte, R. J.; Wang, Q.; Eisenberg, R. *Inorg. Chem.* **2005**, *44*, 2628. (b) Chakraborty, S.; Wadas, T. J.; Hester, H.; Schmehl, R.; Eisenberg, R. *Inorg. Chem.* **2005**, *44*, 6865. (c) Chakraborty, S.; Wadas, T. J.; Hester, H.; Flaschenreim, C.; Schmehl, R.; Eisenberg, R. *Inorg. Chem.* **2005**, *44*, 6284.

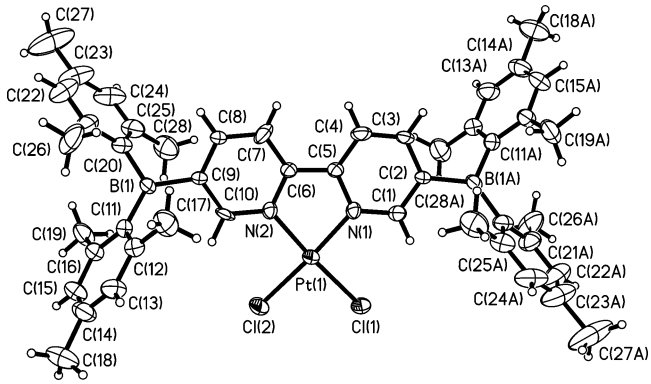

Figure 1. Diagram showing the structure of **Pt-1a** with 35% thermal ellipsoids and labeling schemes.

Figure 2 along with those of the Pt(II) complexes. The absorption bands at $\lambda > 300$ nm are listed in Table 1. The λ_{max} of the low energy absorption band for the free ligands follows the order of B2bpy (350 nm) < N2bpy (381 nm) < BNbpy (400 nm) in CH_2Cl_2, which accounts for their color difference (colorless, pale yellow, yellow). Among the three ligands, BNbpy has the lowest absorption energy that arises from the N→B charge transfer transition. The absorption spectra of BNbpy show a small red shift with increasing solvent polarity ($\lambda_{max} = 393$ nm in hexanes, 400 nm in CH_2Cl_2) that is consistent with the excited-state being more polarized than the ground state. The trend of the absorption energy for the B2bpy and N2bpy molecules is consistent with $\pi \rightarrow \pi^*$ transitions where electron accepting boron centers in B2bpy clearly widens the $\pi-\pi^*$ gap by greatly stabilizing the highest occupied molecular orbital (HOMO) level while the electron donating nitrogen atoms in N2bpy narrows the $\pi-\pi^*$ gap by mostly destabilizing the HOMO level.

Complexes. Each Pt(II) complex has an absorption band similar to the low energy absorption band of the corresponding free ligand except that the λ_{max} of this band in the complex is red-shifted, an indication that N,N-chelation to the Pt(II) center decreases the $\pi \rightarrow \pi^*$ (or N→B in case of BNbpy) energy, which can be attributed to the enhanced π conjugation of the ligand and the σ donation. Nonetheless, the λ_{max} of this ligand centered band of the $PtPh_2$ complexes follows a different order from that of the free ligands with Pt(B2bpy)Ph_2 (**Pt-1**, 355 nm) < Pt(BNbpy)Ph_2 (**Pt-2**, 430 nm) ≈ Pt(N2bpy)Ph_2 (**Pt-3**, 431 nm) in CH_2Cl_2. This change of ordering is mainly caused by the dramatic red shift of the $\pi \rightarrow \pi^*$ transition band of Pt(N2bpy)Ph_2 (50 nm), that is much greater than that of the $\pi \rightarrow \pi^*$ transition band of Pt(B2bpy)Ph_2 (5 nm) and the N→B charge transfer transition of Pt(BNbpy)Ph_2 (30 nm), relative to the corresponding free ligand. The energy of the same ligand-based band of the $PtCl_2$ complexes Pt(B2bpy)Cl_2, (**Pt-1a**, 369 nm) and Pt(BNbpy)Cl_2, (**Pt-2a**, 455 nm) is further red-shifted, relative to the $PtPh_2$ analogues, supporting that the auxiliary ligands on the Pt(II) center have a significant impact on the N,N-chelate ligand's energy levels. Compared to the free ligands, the Pt(II) complexes have much more intense colors: red (**Pt-1**), light yellow (**Pt-1a**), yellow (**Pt-2**), yellow-orange (**Pt-2a**), yellow (**Pt-3**) in solution (CH_2Cl_2). While the distinct red color of **Pt-1** is clearly caused by the weak but well-resolved MLCT absorption band at 525 nm ($\varepsilon = 1390$ M^{-1} cm^{-1}), the color displayed by the other Pt(II) complexes may be attributed to both $\pi \rightarrow \pi^*$ (or N→B) absorption band of the chelate ligand and the MLCT band because these two bands overlap and are not resolved in the absorption spectra. Nonetheless, the absorption spectral data support unambiguously that the MLCT energy of complex **Pt-1** is much lower than all other Pt(II) complexes among this group. The two boron centers and the phenyl auxiliary ligands in **Pt-1** clearly play a key role in promoting such a low energy MLCT transition by stabilizing the π^* level and enhancing the Pt(II) d energy level (HOMO). The $PtMe_2$ analogue[8] of **Pt-1** displays a similar MLCT band at $\lambda = 550$ nm. The red shift of the MLCT energy from Pt(B2bpy)Ph_2 to Pt(B2bpy)Me_2 is consistent with the greater σ donating ability of methyl that increases the d (HOMO) level, relative to phenyl, thus decreasing the MLCT energy. It is noteworthy that the MLCT band of Pt(B2bpy)Ph_2 and Pt(B2bpy)Me_2 experiences a blue shift with increasing solvent polarity, consistent with the excited-state of these Pt(II) complex being less polarized than the ground state.[11] To verify the impact of Pt(II) chelation and the auxiliary ligands on the π^* (LUMO) energy level and the electron accepting ability of the boron center in the complexes, the electrochemical properties of the free ligands and their complexes were examined.

Electrochemical Properties. Ligands. The reduction potentials of the free ligands and the Pt(II) metal complexes were recorded by cyclic voltammetry. For comparison, 2,2′-bpy and Pt(bpy)Ph_2 were also examined by CV. The reduction potentials are shown in Table 2 and Figure 3. N2bpy and 2,2′-bpy do not display any reversible reduction peaks under the experimental conditions we used (DMF as the solvent, NBu_4PF_6 as the electrolyte). The BNbpy molecule has one reversible reduction peak at −1.99 V (vs $FeCp_2^{0/+}$), which is much more positive than that of B(Mes)$_2$-biphenyl-NPh(1-naph) (BNPB, −2.36 V). The greater electron accepting ability of BNbpy, compared with that of BNPB, can be attributed to the greater π conjugation, caused by the electronegative nitrogen atom and the greater coplanarity of the two py rings in BNbpy. For the diboron B2bpy molecule, two reversible reduction peaks at −1.69 and −2.04 V, respectively, were observed, which may be attributed to the sequential reduction of the two boron centers. The $E_{1/2}^{red1}$ of B2bpy is about 0.30 V more positive than that of BNbpy, supporting that the second boron center in B2bpy can greatly enhance the electron accepting ability of the molecule via π conjugation with the first boron center through the bpy linker. Again, the two reduction potentials, $E_{1/2}^{red1}$ and $E_{1/2}^{red2}$ of B2bpy are much more positive than those of B(Mes)$_2$-biphenyl-BMes$_2$, further supporting the effectiveness of the bpy linker in enhancing the electron accepting ability of the boron center. Notably neither BNbpy nor N2bpy display reversible oxidation peaks, which is in

(12) (a) King, K. A.; Spellane, P. J.; Watts, R. J. *J. Am. Chem. Soc.* **1985**, *107*, 1431. (b) Lamansky, S.; Djurovich, P.; Murphy, D.; Abdel-Razzaq, F.; Kwong, R.; Tsyba, I.; Bortz, M.; Mui, B.; Bau, R.; Thompson, M. E. *Inorg. Chem.* **2001**, *40*, 1740.

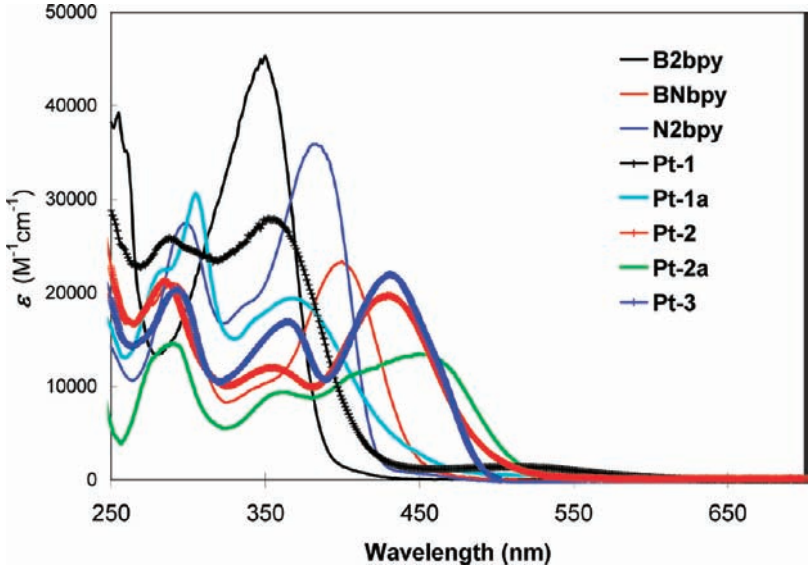

Figure 2. UV−vis absorption spectra of free ligands and their Pt(II) complexes recorded in CH_2Cl_2.

Table 1. Absorption and Luminescence Data

compd	UV−vis, nm (ε, M^{-1} cm^{-1})	λ_{em}, nm/ τ^c, μs CH_2Cl_2, rt	λ_{em}, nm /τ, ms CH_2Cl_2, 77 K	ϕ^a Neat Film	ϕ^b CH_2Cl_2
B2bpy	350 (41,518)	430	489/2.7(2)	<0.01	0.01
BNbpy	400 (23,378)	501	538/5.9(1)	0.15(2)	0.95
N2bpy	381 (35,870)	428	548/2.6(1)	0.05(2)	0.76
Pt-1	355 (28,000),525 (1,390)	N/A	515/0.49(1)	N/A	N/A
Pt-1a	369 (19,387)	N/A	535/0.0253(1) 0.238(1)	N/A	N/A
Pt-2	356 (11,968), 430 (19,687)	565/6.80(1)	597/0.52(1)	<0.01	0.0007
Pt-2a	360 (9,371), 455 (13,455)	591/8.40(1)	634/0.0258(1)	N/A	0.0002
Pt-3	363 (16,903),431(21,967)	510/2.3(1), 7.8(1)	565/0.40(1)	<0.01	0.0058

[a] Quantum efficiency obtained using an integration sphere spectrometer. [b] The quantum efficiency for the free ligands was obtained under air using 9,10-diphenylanthracene as the standard. For the Pt(II) complexes, the quantum efficiency was measured under N_2 using $Ir(ppy)_3$ as the standard (Φ = 0.40).[12] The relative quantum efficiencies of complexes **Pt-2**, **Pt-2a**, and **Pt-3** versus $Ir(ppy)_3$ under air are 0.22, 0.022 and 1.07, respectively. [c] The decay lifetime at r.t. for the Pt(II) complexes was measured under N_2 and air, respectively. Similar lifetimes were observed under either N_2 or air. The numbers in the table were obtained under N_2.

Table 2. Electrochemical Data[a]

	$E_{1/2}^{red1}$ (V)	$E_{1/2}^{red2}$ (V)	ΔE (V)
B2bpy	−1.69	−2.04	0.35
Pt-1	−1.34	−1.73	0.39
Pt(B2bpy)Me_2	−1.38	−1.76	0.38
Pt-1a	−1.17	−1.54	0.37
BNbpy	−1.99		
Pt-2	−1.62	−2.10	0.48
Pt-2a	−1.40	−1.84	0.44
Pt-3	−1.99		
Pt(bpy)Ph_2	−1.93		

[a] All potentials are relatively to $FeCp_2^{0/+}$, measured in DMF, using NBu_4PF_6 as the electrolyte with scan rates 100 mV to 1000 mV.

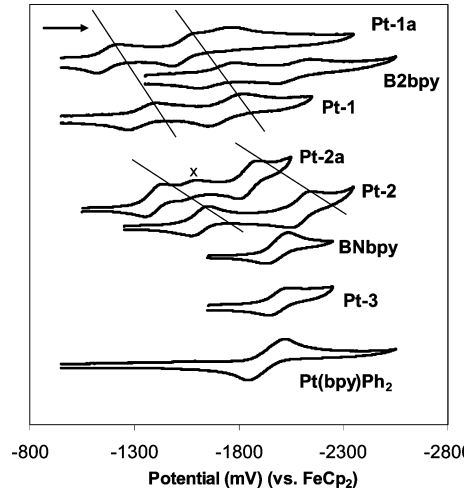

Figure 3. CV diagrams for the Pt(II) complexes recorded in DMF and the free ligands B2bpy and BNbpy. Note: Pt(BNbpy)Cl_2 has a poor solubility and its CV spectrum was recorded at a very low concentration, as a consequence, the impurity peak at ~−1.5 V from the electrolyte became significant.

sharp contrast to BNPB and NPB ((1-naph)PhN-biphenyl-NPh(1-naph)) molecules, both of which display reversible oxidation peaks ($E_{1/2}^{ox}$ = 0.55 V for BNPB, $E_{1/2}^{ox1}$ = 0.25 V for NPB),[2f,g] that are typical of triarylamino groups. Hence, the bpy linker decreases the electrochemical stability of the amino group in BNbpy and N2bpy toward oxidation, which is not surprising since its electron withdrawing nature destabilizes the radical cation, relative to a phenyl or biphenyl.

Pt(II) Complexes. Like B2bpy, Pt(B2bpy)Ph_2, Pt(B2bpy)-Me_2, and Pt(B2bpy)Cl_2 display two reversible reduction peaks that are more positive than those of B2bpy by 0.30−0.52 V. The great enhancement of the electron accepting ability of the Pt(II) complexes can be attributed to the donation of the lone pair electrons of B2bpy to the metal center that reduces the electron density on the ligand, thus increasing its electron accepting ability, and the increased π-conjugation that effectively lowers the π^* level. Among the three B2bpy complexes, the $PtMe_2$ compound has the most negative reduction potentials while the $PtCl_2$

Table 3. HOMO and LUMO Energy and Gap of Ligands and Complexes

	experimental energy/eV			calculated energy/eV		
	HOMO[c]	LUMO[a]	energy gap[b]	HOMO	LUMO	energy gap
B2Bbpy	−6.22	−3.11	3.11	−6.25	−2.44	3.81
BNbpy	−5.39	−2.81	2.58	−5.37	−2.15	3.22
N2bpy	−5.46[d]	−2.58[e]	2.88	−5.10	−1.48	3.62
Pt-1	−5.46	−3.46	2.00	−5.11	−2.98	2.13
Pt-2	−5.58	−3.18	2.40	−5.06	−2.62	2.44
Pt-3	−5.27	−2.81	2.46	−5.02	−2.15	2.87
Pt-1a	−6.11	−3.63	2.48	−5.91	−3.37	2.54
Pt-2a	−5.70	−3.40	2.30	−5.80	−2.98	2.82
Pt(bpy)Ph$_2$	−5.21	−2.87	2.34			

[a] From the reduction potential in DMF. [b] From absorption edge of the UV−vis spectrum. [c] Calculated from experimental LUMO and the HOMO−LUMO gap. [d] From the oxidation potential in DMF. [e] From the experimental HOMO and the HOMO−LUMO gap.

one has the most positive reduction potential ($E_{1/2}^{red1} = -1.17$ V, $E_{1/2}^{red2} = -1.54$ V), which is consistent with the much weaker *trans* effect of the chloride ligand, relative to the phenyl or methyl ligand, that leads a stronger B2bpy binding to the Pt(II) center in **Pt-1a**, as supported by the crystal structural data. It is noteworthy that both $E_{1/2}^{red1}$ and $E_{1/2}^{red2}$ of the B2bpy complexes are much more positive than that of Pt(bpy)Ph$_2$ (one reduction peak at −1.93 V). For **Pt-1a**, a third reduction peak at ∼1.8 V is also observed, which may be attributed to the reduction of the bpy ring. Pt(N$_2$bpy)Ph$_2$, (**Pt-3**) displays a reversible reduction peak at −1.99 V, that is somewhat more negative than that of Pt(bpy)Ph$_2$ and attributed to the reduction of the bpy ring, supporting that the electron donating NPh$_2$ group of N2bpy indeed destabilizes the lowest unoccupied molecular orbital (LUMO) level of the **Pt-3** complex, relative to the bpy complex. Both **Pt-2** and **Pt-2a** display two reversible reduction peaks that are far apart ($\Delta E = 0.48$ and 0.44 V, respectively). On the basis of the CV data of the B2bpy and N2bpy complexes, the two reduction peaks of the BNbpy complexes **Pt-2** and **Pt-2a** can be assigned to the reduction of the boron center and the bpy ring, respectively. Again, the reduction potentials of the chloride complex **Pt-2a** are much more positive than those of the phenyl analogue **Pt-2**, consistent with the trend observed for the B2bpy complexes **Pt-1** and **Pt-1a**. The $E_{1/2}^{red1}$ potentials of the BNbpy cmplexes are all much more positive than the free ligand, again supporting that chelation to the Pt(II) center enhances the electron accepting ability of the boron center. Interestingly, the magnitude of the $E_{1/2}^{red1}$ potential shift from the free ligands to the Pt(II) complexes is nearly identical for both B2bpy and BNbpy systems. On the basis of the CV data, the electron accepting ability of the complexes and the ligands follows the order of **Pt-1a** > **Pt-1** > Pt(B2bpy)Me$_2$ > **Pt-2a** > **Pt-2** > B2bpy > Pt(bpy)Ph$_2$ > **Pt-3** ≈ BNbpy. Hence, the ability of the boron center in the metal complexes and the free ligands to bind to anions such as fluoride is expected to follow the order of **Pt-1a** > **Pt-1** > Pt(B2bpy)Me$_2$ > **Pt-2a** > **Pt-2** > B2bpy > BNbpy.

Using the CV and UV−vis data, the HOMO and LUMO energies of the ligands and their complexes were obtained and shown in Table 3 and Figure 4. The data show consistently the stabilization of the LUMO level of B2bpy and BNbpy by metal chelation, and the significant impact of the different bpy chelate ligands and the auxiliary ligands on the HOMO energy level. For the chloride auxiliary ligand, the B2bpy complex **Pt-1a** has a much lower HOMO than that of the BNbpy complex **Pt-2a**, while the opposite is observed for **Pt-1** and **Pt-2** that contain the phenyl ligands. For the B2bpy chelate ligand, the HOMO level of the complexes increases in the order of $Cl^- < Ph < Me$, which is consistent with the HOMO level being dominated by the Pt(II) d orbital that is destabilized by strong σ auxiliary ligands such as a methyl. Also notable is that the HOMO energy difference between the BNbpy complexes **Pt-2** and **Pt-2a** is much less pronounced than that of the B2bpy complexes **Pt-1** and **Pt-2**.

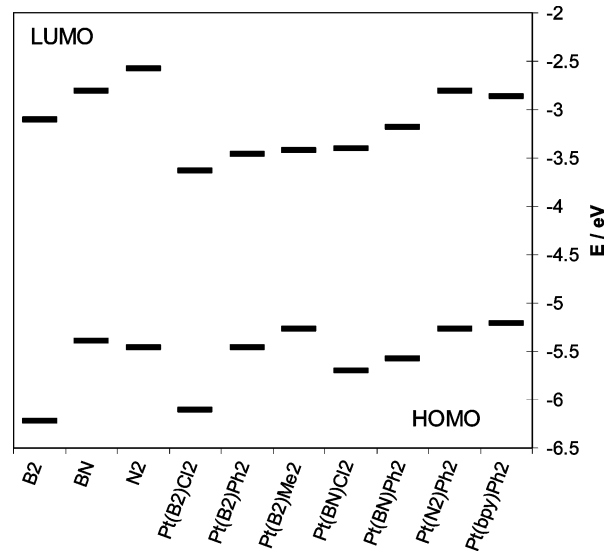

Figure 4. HOMO and LUMO energy levels of free ligands and Pt(II) complexes obtained from CV and UV−vis data (see Table 3).

Luminescence. Ligands. The luminescent properties of the free ligands and their complexes were examined by fluorescent and phosphorescent spectra. Under UV irradiation, all three free ligands display luminescence in solution (CH_2Cl_2) at ambient temperature: a weak blue emission for B2bpy ($\lambda_{em} = 430$ nm, $\Phi = 0.01$), a bright green emission for BNbpy ($\lambda_{em} = 501$ nm, $\Phi = 0.95$), and a bright blue emission for N2bpy ($\lambda_{em} = 427$ nm, $\Phi = 0.76$), with the donor−acceptor compound BNbpy having the lowest emission energy and the highest emission quantum efficiency. The emission band of BNbpy has a strong dependence on the solvent polarity with λ_{max} shifting from 434 nm in hexanes to 552 nm in CH_3CN (Figure 5), confirming the presence of a highly polarized excited-state and the charge transfer nature of the emission. In the solid state, B2bpy has no visible emission while BNbpy and N2bpy emit a bright blue-green color at 483 nm ($\Phi = 0.15$, measured by integration sphere methods) and 495 nm ($\Phi = 0.05$), respectively. The ∼65 nm red shift by N2bpy from solution to the solid state is likely caused by intermolecular π stacking interactions in the solid state.

Complexes. The luminescent property of Pt(B2bpy)Me$_2$ was not investigated because of its poor stability in solution. **Pt-1** and **Pt-1a** have no detectable luminescence in solution

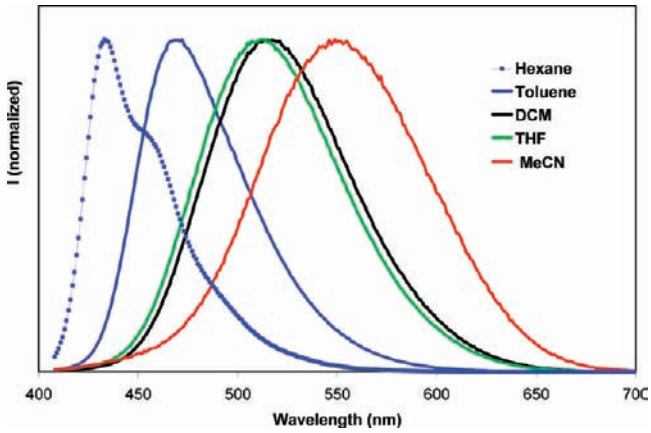

Figure 5. Emission spectra of BNbpy in different solvents, [BNbpy] = $\sim 1.0 \times 10^{-5}$ M.

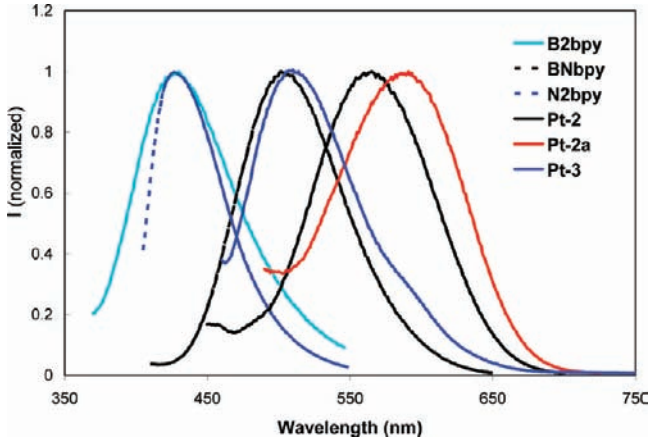

Figure 6. Emission spectra of B2bpy, BNbpy, **Pt-2**, **Pt-2a**, and **Pt-3** in CH_2Cl_2, 1.0×10^{-5} M, r.t. under air.

at ambient temperature while **Pt-2** and **Pt2a** display an orange and a red-orange phosphorescent emission with λ_{max} = 565 nm, τ = 6.80 (2) μs; and 591 nm, τ = 7.70(2) μs, respectively, in CH_2Cl_2 under air (Figure 6). The order of the emission energy of **Pt-2** and **Pt-2a** follows that of the low energy absorption band of the two complexes and may be attributed to either a BNbpy centered B→N charge transfer transition or MLCT transitions. However, since the auxiliary ligands phenyl and chloride have no significant impact on the HOMO level of **Pt-2** and **Pt-2a**, as shown in Figure 4 and Table 3, the HOMO level of these two complexes is likely dominated by the π orbital of BNbpy. Consequently, the emission of **Pt-2** and **Pt-2a** is most likely from ligand centered B→N charge transfer transitions. The N2bpy complex **Pt-3** emits a blue color with λ_{max} = 510 nm, τ = 2.3(1) μs, 7.8(1) μs in CH_2Cl_2 at ambient temperature, which is likely from a ligand-based transition as well. At 77 K, in frozen CH_2Cl_2, all Pt(II) complexes display phosphorescence with long decay lifetimes as shown in Table 1. Compared to the 77 K emission spectra of the corresponding free ligands, the spectra of the complexes are all red-shifted considerably (see Table 1). The phosphorescent decay lifetimes of the complexes at 77 K are all much shorter than those of the free ligands (2.6−5.9 ms), consistent with the heavy atom effects in the complexes. In the solid state, at ambient temperature, **Pt-1** and **Pt-1a** have no detectable emission while **Pt-2** and **Pt-3** emit a weak red and a red-orange color with λ_{max} at 647 and 594 nm, respectively. To verify that the solid state emission is from intramolecular transitions, we measured the emission spectra of **Pt-2** and **Pt-3** doped in a PMMA matrix (10% by weight, PMMA = poly(methyl methacrylate) at ambient temperature. The PMMA film of **Pt-3** displays a phosphorescent peak with λ_{max} = 591 nm (τ = 9.61(3) μs) that resembles the solid state emission spectrum. The **Pt-2** PMMA film displays two emission peaks at λ = 498 and 585 nm, respectively, with the former being fluorescent, attributable to B→N charge transfer, and the latter being phosphorescent (τ = 11.29(4) μs), similar to that of the frozen solution at 77 K, but much blue-shifted, compared to that of the solid at ambient temperature. Hence, the solid state emission spectrum of **Pt-2** can be attributed to intermolecular interactions.

Density Functional Theory (DFT) Calculations. To better understand the photophysical properties of the complexes, DFT calculations for the three free ligands and their $PtPh_2$ complexes were performed. The geometric parameters from X-ray diffraction analysis were used initially and further optimized for the calculations for B2bpy, **Pt-1**, and **Pt-1a**. For all other compounds, geometric parameters were obtained by molecular modeling and geometry optimization. The Gaussian suite of programs[13] (Gaussian 03, basis set B3LYP-6-311G) was employed for the calculations. The calculated HOMO and LUMO energy levels and the energy gaps for the ligands and the complexes are provided in Table 3. The HOMO and LUMO orbitals of the free ligands and the $PtPh_2$ complexes and **Pt-2a** are shown in Figures 7 and 8 (the diagrams for **Pt-1a** are provided in Supporting Information), respectively.

The HOMO level for B2bpy is mainly from the mesityls while the LUMO level is a π^* orbital dominated by the two boron atoms and the bpy unit; hence, the lowest electronic transition of B2bpy can be considered as mesityls to the B-bpy-B unit charge transfer. The HOMO level of BNbpy involves the bpy unit and the NPh_2 group while the LUMO is dominated by the B atom with significant contributions from the bpy, supporting that the lowest electronic transition of BNbpy is charge transfer from NPh_2 to the boron center, mediated by the bpy unit via π-conjugation. For N2bpy, the HOMO level is a π orbital involving the entire molecule while the LUMO level is a π^* orbital dominated by the bpy unit. Hence, the lowest electronic transition of N2bpy is a $\pi \rightarrow \pi^*$ transition. The general trend is that both HOMO and LUMO levels increase in the order of B2bpy < BNbpy < N2bpy with B2bpy displaying the most pronounced HOMO stabilization while the N2bpy displaying the most LUMO destabilization, consistent with the experimental data shown in Figure 3. The overall calculated HOMO−LUMO energy gap follows the order of BNbpy < N2bpy < B2bpy, in agreement with the trend observed experimentally.

As shown in Figure 8, the HOMO level for the three $PtPh_2$ complexes consists of π orbitals of the two phenyl group and the d orbital of the Pt(II) center, with the energy varying slightly (**Pt-1** < **Pt-2** < **Pt-3**). In contrast, the LUMO level of each complex is quite distinctive and closely resembles

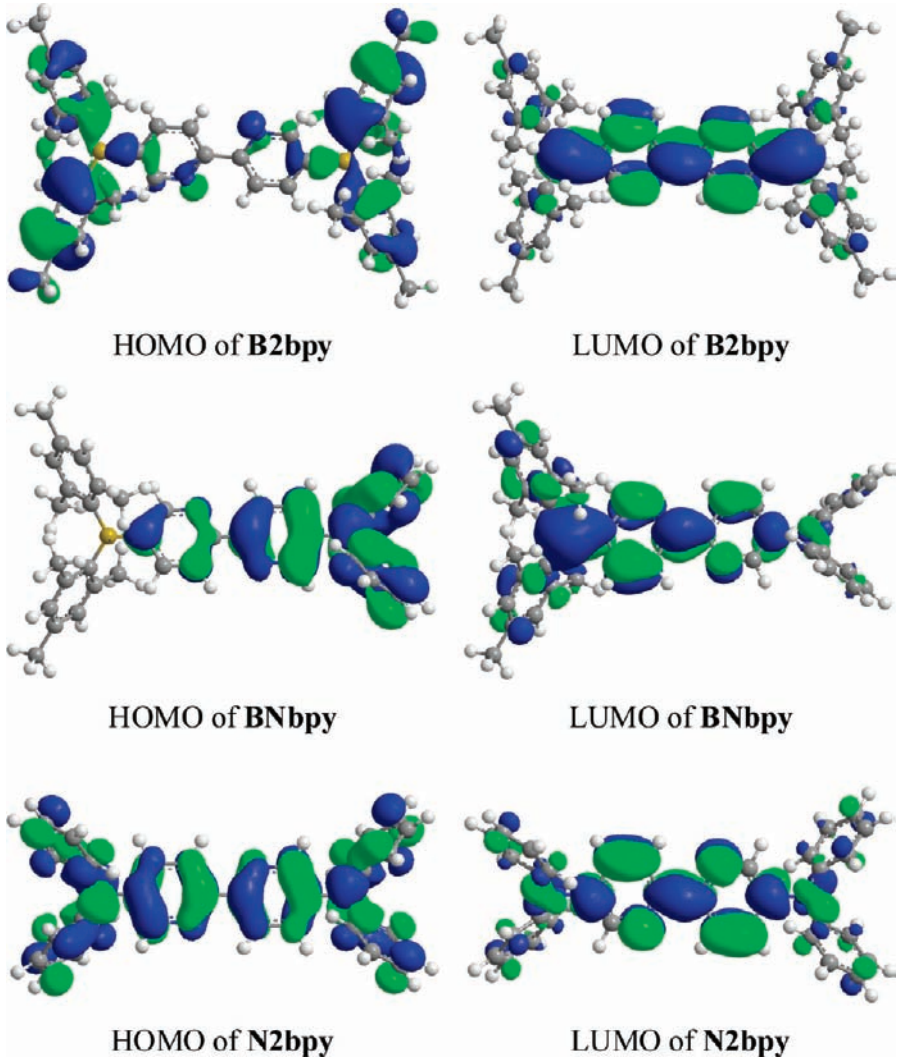

Figure 7. HOMO and LUMO orbitals of B2bpy, BNbpy, and N2bpy plotted with a 0.02 iso-contour value.

that of the corresponding free ligand. For example, the LUMO of **Pt-1** is a π^* orbital of the B2bpy ligand with some contributions of a d orbital from the Pt(II) center as part of the π-conjugation. The LUMO levels of **Pt-2** and **Pt-3** also exhibit similar d orbital contributions from the Pt(II) center. Hence, the lowest electronic transition of the three $PtPh_2$ complexes can be indeed considered as charge transfer from $PtPh_2$ to the π^* orbital of B2bpy, BNbpy, and N2bpy, respectively. The DFT results also show that the HOMO energy does not change significantly among the three $PtPh_2$ complexes while the LUMO energy varies quite dramatically with **Pt-1** having the deepest LUMO (−2.98 eV) and **Pt-3** the highest LUMO (−2.15 eV), and as a consequence, the HOMO−LUMO gap follows the order of **Pt-1** < **Pt-2** < **Pt-3**, which agrees well with the experimental data. For the two $PtCl_2$ complexes, **Pt-1a** and **Pt-2a**, the HOMO level consists of the Pt d orbital and the lone pair orbitals of the Cl^- ligands while the LUMO level resembles that of the $PtPh_2$ analogues. The computational results show that the HOMO and LUMO energies of **Pt-1a** and **Pt-2a** are much lower than those of **Pt-1** and **Pt-2** and that the impact of the auxiliary ligand phenyl and chloride is most pronounced at the HOMO level, a trend again consistent with the experimental data.

Response to Fluorides. One unique feature of the B2bpy and BNbpy Pt(II) complexes that distinguishes them from previously known push−pull Pt(II) complexes is the presence of a three-coordinate boron center capable of selective binding to anions such as fluorides and cyanides.[3,4] This feature can not only be exploited for anion sensing but more importantly can be used to probe the various electronic transition pathways such as MLCT and the Lewis acidity of the boron center in the complexes. We therefore examined and compared the response of B2bpy, BNbpy, and their Pt(II) complexes toward fluoride ions in both UV−vis and fluorescent modes.

B2bpy and BNbpy. As demonstrated previously, B2bpy undergoes sequential addition of F^- with the formation of $B2bpyF^-$ being quantitative and the need of ∼2 equiv of F^- for the formation of $B2bpyF_2^{2-}$ with K_1 and K_2 being $\geq 10^8$ M^{-1} and $\sim 10^6$ M, respectively. The binding strength of the BNbpy to F^- is similar to that of $B2bpyF^-$, as supported by the similar UV−vis spectral change and the Stern−Volmer plots (Figure 9 and Supporting Information). The most interesting contrast between B2bpy and BNbpy is their fluorescent spectral change upon binding with fluorides as shown in Figure 9. For B2bpy, the addition of F^- causes a

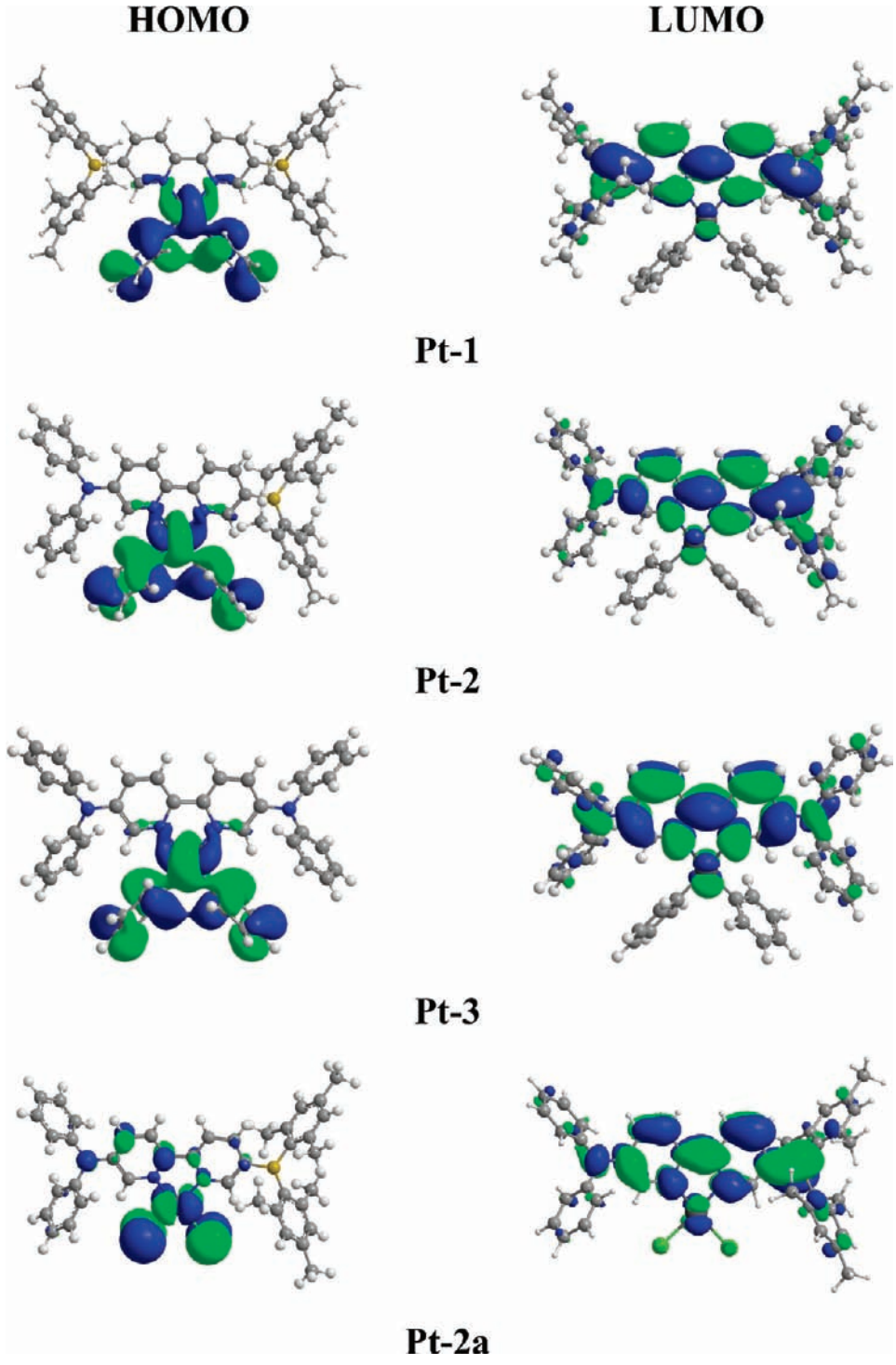

Figure 8. HOMO and LUMO orbitals of **Pt-1**, **Pt-2**, **Pt-3**, and **Pt-2a** plotted with a 0.02 iso-contour value.

partial quenching and a small red shift of the emission peak. For BNbpy, the addition of F^- causes a complete quenching of the emission peak at 501 nm, accompanied by the appearance and a rapid increase of a new emission peak at 400 nm, resulting in the emission color switch from blue-green to deep blue. Therefore, BNbpy can be described as a fluorescent turn-on sensor toward fluorides while B2bpy a turn-off sensor. The new emission band at 400 nm of $BNbpyF^-$ may be attributed to a $\pi \rightarrow \pi^*$ transition of the adduct. The "turn-on" response of BNbpy is rare for conjugated donor−acceptor triarylboron systems[3,4] and is in sharp contrast to the biphenyl analogue, BNPB, which has the N→B charge transfer emission energy at ~440 nm about 60 nm blue-shifted, compared to that of BNbpy and undergoes a straight fluorescent quenching upon the addition of fluoride ions.[4d,e] The emission quenching of BNPB by fluoride can be explained by the fact that the $\pi \rightarrow \pi^*$ emission energy of the fluoride adduct $BNPBF^-$ is in the same region as that of the BNPB charge transfer but has a much lower quantum efficiency because of the lack of coplanarity of the biphenyl group. In contrast, the unusual "turn-on" behavior of BNbpy can be explained by the large energy separation

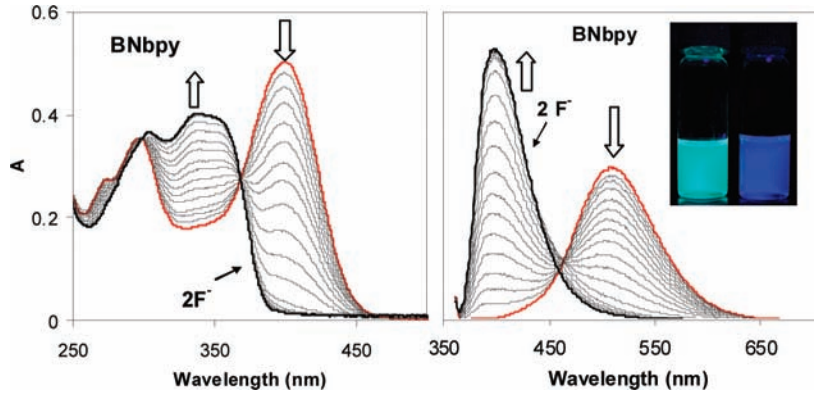

Figure 9. UV−vis (left) and fluorescent (right) spectral change of BNbpy (~1.0×10^{-5} M) with the addition of NBu_4F (λ_{ex} = 350 nm). Inset: Photographs of the BNbpy solution before (left) and after (right) F^- under UV irradiation (lamp wavelength 365 nm).

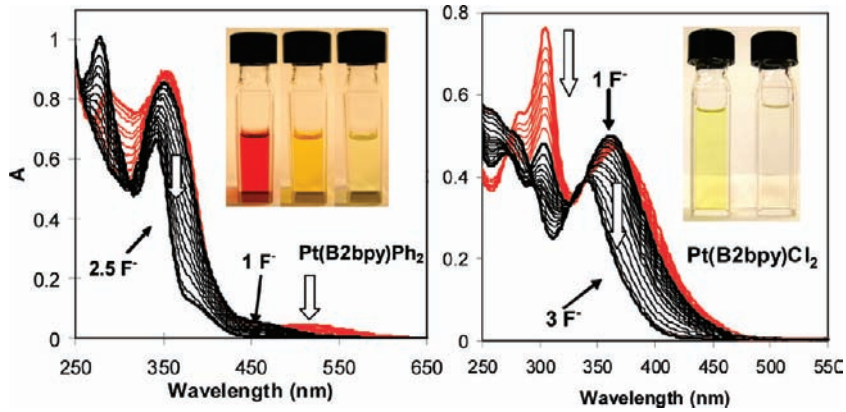

Figure 10. UV−vis spectral change of **Pt-1** (left) and **Pt-1a** (right) with the addition of NBu_4F in CH_2Cl_2. The red region shows the spectral change after 1 equiv of F^-. Inset: photographs showing the color change before (left) and after (right) NBu_4F.

between the N→B charge transfer band of BNbpy and the $\pi \rightarrow \pi^*$ band of $BNbpyF^-$, and the relatively high emission quantum efficiency of $BNbpyF^-$, for which the bpy linker in BNbpy is responsible by lowering the LUMO level and enhancing the coplanarity of BNbpy via hydrogen bonding between the two pyridyl rings. For B2bpy, its emission band is in the same region as those of $B2bpyF^-$ and $B2bpyF^{2-}$, with the latter still having a fairly high emission intensity; thus, the addition of F^- only led to partial quenching of the B_2bpy emission peak.

Pt(B2bpy)Ph_2 and Pt(B2bpy)Cl_2. As described in the preliminary communication, the addition of F^- to the solution of **Pt-1** in CH_2Cl_2 causes a sequential quenching of the MLCT absorption because of the stepwise formation of the 1:1 and 2:1 fluoride adducts with $K_1 \geq 10^9$ M^{-1} and K_2 = ~10^6 M^{-1} in CH_2Cl_2 and visual stepwise color switching from red to orange to light yellow. The response of **Pt-1a** to fluoride ions is similar to that of **Pt-1** except that the color change is from yellow to colorless because of the blue shift of the MLCT band, as shown in Figure 10 (for comparison, the spectrum of **Pt-1** is also shown). The CV data indicate that **Pt-1a** should have a stronger binding with fluorides than **Pt-1** does. However, because of the strong binding of both complexes with F^-, accurate binding constants that allow direct comparison could not be obtained. Nonetheless, both complexes are capable of binding to one F^- in either THF/ethanol or DMF/H_2O solvent mixtures (see Supporting Information). Although the color change of **Pt-1a** with F^- is not as striking as **Pt-1**, for practical applications, it does have the advantage for being much more stable in alcohol or aqueous solvents than **Pt-1** which slowly decomposes over time. The binding of F^- with **Pt-1** and **Pt-1a** was also confirmed by ^1H and ^{19}F NMR spectra.

Pt(BNbpy)Ph_2 and Pt(BNbpy)Cl_2. As shown in Figure 11, the absorption spectral change of **Pt-2** and **Pt-2a** with the addition of F^- resembles that of [(**Pt-1**)F^-] and [(**Pt-1a**)F^-], respectively, with quenching and a blue shift of the low energy absorption band. The color of these two complexes changes from light yellow and yellow to colorless and light yellow, respectively, with fluoride. The binding constants with fluoride for these two complexes were estimated to be ~7.0×10^5 M^{-1} and 5.0×10^6 M^{-1}, respectively, with **Pt-2a** having a stronger binding constant.

The key advantage of the BNbpy complexes over the B2bpy ones is their luminescence at ambient temperature under air, enabling the detection of the fluoride binding event by fluorescent spectroscopy. As shown by the photographs and the fluoride titration diagrams in Figure 12, the addition of fluoride ions to the solution of **Pt-2** or **Pt-2a** causes the emission color switching from orange or red-orange to bright whitish blue-green, with the emission λ_{max} change from 565 to 485 nm for **Pt-2**, and 591 to 510 nm for **Pt-2a** and a great gain of emission intensity (This "turn-on" phenomenon is persistent with λ_{ex} = 400−430 nm for **Pt-2**, 430−470 nm for **Pt-2a**.). The saturation point is reached after the addition of ~1.5 equiv of F^- for both compounds. The "turn-on"

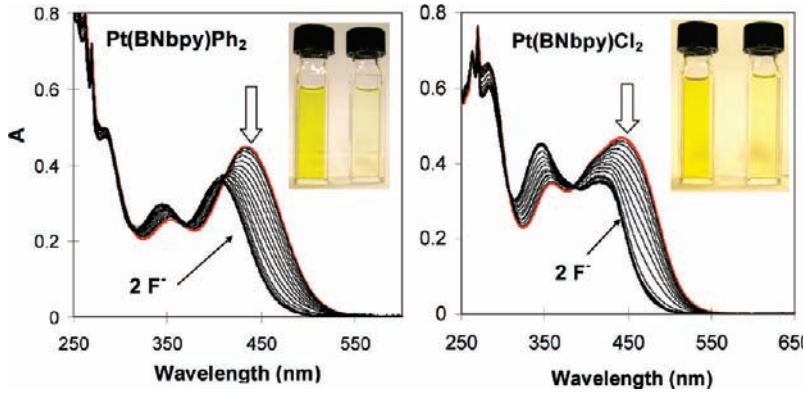

Figure 11. UV−vis spectral change of **Pt-2** (left) and **Pt-2a** (right) with the addition of NBu_4F in CH_2Cl_2. Inset: photographs showing the absorption color change before (left) and after (right) F^-.

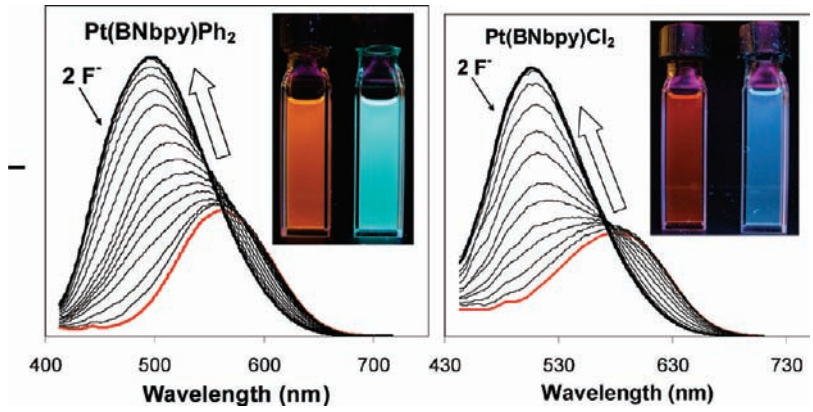

Figure 12. Fluorescent spectral change of **Pt-2** (left, λ_{ex} = 400 nm) and **Pt-2a** (right, λ_{ex} = 430 nm) (~1.0×10^{-5} M) with the addition of NBu_4F in CH_2Cl_2. Inset: photographs of the solution of the metal complexes at the titration concentration before (left) and after (right) F^- under UV irradiation (lamp wavelength 365 nm).

luminescent spectral change of **Pt-2** and **Pt-2a** resembles that of the free BNbpy ligand except that compared to BNbpy, the emission peaks of **Pt-2**, **Pt-2a**, and their fluoride adducts are all at much longer wavelengths. Hence, the "turn-on" response of **Pt-2** and **Pt-2a** toward fluoride may have the same origin as the BNbpy free ligand, namely, a switching from a N→B charge transfer (with possible MLCT contributions) to a $\pi \rightarrow \pi^*$ transition in the fluoride adduct. The role of the Pt(II) center is shifting the emission band to a lower energy by enhancing the π-conjugation of the BNbpy ligand. Metal complexes that respond to fluoride ions in the luminescent mode at ambient temperature under air are rare, and only a few examples of Ir(III) complexes based the ppy ligand have been reported recently.[6b,c] What distinguish the Pt(II) BNbpy complexes from other complexes are their distinct color switch and the great emission intensity gain upon the addition of fluoride.

Conclusions

A new class of 2,2′-bipyridyl supported conjugated system that contains either two $BMes_2$ acceptor groups, or two NPh_2 donor groups, or a $BMes_2$ and a NPh_2 donor−acceptor groups has been developed. The acceptor-only molecule B2bpy has the highest electron affinity while the donor−acceptor molecule BNbpy has the lowest HOMO−LUMO gap and the highest emission quantum efficiency with a unique fluorescent "turn-on" response toward fluoride ions mediated by the bipy unit. The 2,2′-bipy unit greatly enhances the electron-accepting ability of the triarylboron center by stabilizing the radical anion, compared to a biphenyl unit. For the donor-only molecule, the 2,2′-bipy unit reduces the electron donating ability of the amino center by destabilizing the radical cation. Chelation by a Pt(II) center to these new ligands has been found to greatly enhance the electron accepting ability via both σ donation and increased π-conjugation. The auxiliary ligands on the Pt(II) center have also been found to have a significant impact on the electron affinity of the 2,2′-bipy derivative ligands with the chloride complexes having the deepest LUMO level, and thus the strongest electron acceptor. Furthermore, chelation by a Pt(II) ion reduces the HOMO−LUMO gap dramatically, compared to the free ligand, because of the participation of the Pt(II) d orbital and the auxiliary ligand at the HOMO level and the enhanced π conjugation of the ligand. As a result, the Pt(II) complexes can detect fluoride ions with a distinct color change by either absorption or emission in the visible region. Significantly the Pt(II) complexes of BNbpy and N2bpy all display room-temperature phosphorescence in solution under air that is most likely dominated by BNbpy or N2bpy ligand-centered transitions. The phosphorescent emission of $Pt(BNbpy)Ph_2$ and $Pt(BNbpy)Cl_2$ has a dramatic "turn-on" response toward fluoride ions with color switch from orange or red-orange to whitish blue-

green, attributed to switching from a N→B charge transfer transition to a $\pi \rightarrow \pi^*$ transition on the BNbpy ligand. The persistent "turn-on" response toward fluoride ions by the free BNbpy ligand and its Pt(II) complexes can be explained by the large emission energy difference between the fluoride-bound and the non-bound states of the molecule and the high degree of π-conjugation of the BNbpy ligand promoted by the bipy unit and metal chelation. Thus, the new 2,2′-bipy supported conjugated ligand system is not only useful in achieving potentially highly emissive ambient temperature phosphorescent metal complexes but also very promising as a new class of highly effective "turn-on" visual color sensors for fluoride ions in both absorption and emission modes.

Acknowledgment. We thank the Natural Sciences and Engineering Research Council of Canada for financial support and Dr. Rui-Yao Wang for his assistance in the structural refinement of **Pt-1a**.

Supporting Information Available: UV−vis or fluorescent spectra in different solvents (BNbpy, **Pt-2**, **Pt-3**), low temperature and solid state emission spectra of ligands and complexes, the emission spectra of **Pt-2**, **Pt-2a**, and **Pt-3** recorded under N_2 and air, respectively, UV−vis and fluorescent titration spectra of B2bpy by NBu_4F in CH_2Cl_2, UV−vis titration spectra of **Pt-1a** in 1:1 CH_2Cl_2/MeOH by NBu_4F, luminescent titration spectra of **Pt-2** and **Pt-2a** by NBu_4F using 430 and 450 nm excitation energy, respectively, the binding constant fitting data for BNbpy, **Pt-2**, and **Pt-2a** with fluorides, HOMO and LUMO diagrams of **Pt-1a**, complete crystal structural data of **Pt-1a**. This material is available free of charge via the Internet at http://pubs.acs.org.

IC9000335

(13) Frisch, M. J. et al. *Gaussian 03*, Revision C.02; Gaussian, Inc.: Wallingford, CT, 2004.